Lightning: Principles, Instruments and Applications

Hans Dieter Betz · Ulrich Schumann ·
Pierre Laroche
Editors

Lightning: Principles, Instruments and Applications

Review of Modern Lightning Research

Springer

Editors
Prof. Dr. Hans Dieter Betz
Physics Department
University of Munich
Am Coulombwall 1
85748 Garching
Germany
hans-dieter.betz@abs.de

Prof. Dr. Ulrich Schumann
Deutsches Zentrum für
Luft- und Raumfahrt
Institut für Physik der Atmosphäre
82230 Oberpfaffenhofen
Germany
ulrich.schumann@dlr.de

Prof. Dr. Pierre Laroche
Physics, Instrumentation and Sensing
Department ONERA
29 avenue de la Division
Leclerc, BP 72
92322 Chatillon
France
pierre.laroche@onera.fr

ISBN: 978-1-4020-9078-3 e-ISBN: 978-1-4020-9079-0

Library of Congress Control Number: 2008937155

Cover images (from left to right): Photograph of lightning flash triggered at camp Blanding, Florida (courtesy of University of Florida Lightning Research Group). Radar (second left) and Antenna (background) - courtesy of nowcast GmbH, Munich. Lightning @ 2008 JupiterImages Corporation. Three-dimensional view of a thunderstorm, enabled by the total-lightning capability of LINET (courtesy of nowcast GmbH, Munich).

Printed on acid-free paper

9 8 7 6 5 4 3 2 1

springer.com

Preface

Lightning is a natural phenomenon that has always produced much impact on humans and their societies, mainly because of its impressive appearance and the threats imposed on life and structures. As one consequence, modern lightning research continues to develop effective tools and procedures suited to recognize severe thunderstorms and to generate reliable alert. During the long time of past lightning investigation, much understanding of the discharge processes has been gathered and efficient detection techniques have been implemented. Today, numerous institutions all over the world deal with unraveling the numerous questions about lightning that have remained open, with much success, but as is typical for research in subjects of natural science, the complexity of the phenomena defies fast and comprehensive clarification. Meanwhile, the many competent research efforts and their impressive results render it impossible to present the gathered knowledge in a single book. Thus, the present monograph is designed to describe in 27 chapters merely some of the highlights of current research. Moreover, the topics have been selected to elucidate the lightning phenomena that are readily understandable by a general, educated readership, rather than addressing only specialists in the field. Accordingly, a more deeply interested reader is referred to the ample reports in literature.

At first, the basic phenomenon – the lightning return stroke – is introduced and in the first four chapters, some fundamental charging and discharge mechanisms are illustrated by Baba and Rakov, Rakov, Stolzenburg and Marshall, and Tessendorf. The following five chapters describe lightning detection networks in Europe (Betz et al.), Italy (Biron), Spain (Pineda and Montanya), Australia (Kuleshov et al.), and Brazil (Pinto et al.). Systems that allow mapping of lightning channels are described in two chapters (Defer and Laroche, and Lojou et al.), followed by three chapters that deal with lightning observations from space (Finke, Adamo et al., and Hamlin et al.). Dwyer explains the close coincidence between lightning and high-energy radiation. In the next three chapters the connection between lightning and higher atmosphere effects is depicted, including Schumann resonances that travel around the globe (Satori et al.), and sprites that show up high above thunderclouds (Lyons et al., Farges). The subsequent five chapters describe the relation between lightning and micro-physical parameters (Katsanos et al.), precipitation (Soula), and strong storms (Dombai, Dotzek and Price, Tuomi and Mäkelä). Three chapters are devoted

to climate (Price), and chemistry and climate (Grewe, Pickering et al.). Finally, Loboda summarizes important aspects about lightning protection.

Although current topics of importance are addressed so that the reader receives a quite comprehensive view about the status of modern lightning research, many worthwhile techniques, procedures, and associated aspects are not covered. Nevertheless, the presented material informs about our understanding of the lightning discharge, and works out the many open questions that are often fascinating and deserve future attention.

Hans D. Betz
U. Schumann
P. Laroche

Contents

Contributors

Claudia Adamo Institute of Atmospheric Sciences and Climate, Italian National Research Council, Roma, Italy, c.adamo@isac.cnr.it

Yoshihiro Baba Department of Electrical Engineering, Doshisha University, 1-3 Miyakodani, Tatara, Kyotanabe, Kyoto 610-0321, Japan, ybaba@mail.doshisha.ac.jp

Daniele Biron Centro Nazionale di Meteorologia e Climatologia Aeronautica, Aeroporto Militare "De Bernardis" – Via Pratica di Mare, 45, 00040 Pomezia (RM), Italy, biron@meteoam.it

Steven A. Cummer Duke University, Durham, NC 27708, USA, cummer@ee.duke.edu

Mat Darveniza School of Information Technology and Electrical Engineering, University of Queensland, and Lightning and Transient Protection Pty Ltd, Brisbane, Australia

Eric Defer LERMA-Observatoire de Paris, France, eric.defer@obspm.fr

Nicholas W. S. Demetriades Vaisala Inc, Tucson Operations, 2705 East Medina Road, Tucson, AZ 85706, USA, Nicholas.Demetriades@vaisala.com

Ferenc Dombai Hungarian Meteorological Service, Gilice tér 1. 1156, 1181 Budapest, Hungary, dombai.f@met.hu

Nikolai Dotzek Deutsches Zentrum für Luft- und Raumfahrt (DLR), Institut für Physik der Atmosphäre, Oberpfaffenhofen, 82234 Wessling, Germany, nikolai.dotzek@dlr.de; European Severe Storms Laboratory, Münchner Str. 20, 82234 Wessling, Germany, nikolai.dotzek@essl.org

Joseph R. Dwyer Department of Physics and Space Sciences, Florida Institute of Technology, Melbourne, Florida, USA, jdwyer@fit.edu

Kenneth B. Eack Langmuir Laboratory, New Mexico Institute of Mining and Technology, Socorro, New Mexico, USA

Thomas Farges Commissariat à l'Energie Atomique, Centre DAM-Ile de France, DASE, 91297 Arpajon Cedex, France, thomas.farges@cea.fr

Ullrich Finke University of Applied Sciences and Arts, Ricklinger Stadtweg 120, Hannover, Germany, ullrich.finke@fh-hannover.de

Steve Goodman Center for Satellite Application and Research, NOAA Satellite and Information Service, National Oceanic and Atmospheric Administration, Camp Springs, Maryland, USA

Volker Grewe Deutsches Zentrum für Luft- und Raumfahrt, Institut für Physik der Atmosphäre, Oberpfaffenhofen, 82234 Wessling, Germany, volker.grewe@dlr.de

Timothy Hamlin Space and Remote Sensing Group, ISR-2, Los Alamos National Laboratory, Los Alamos, New Mexico, USA, thamlin@lanl.gov

Ronald L. Holle Vaisala Inc, Tucson Operations, 2705 East Medina Road, Tucson, AZ 85706, USA, Ronald.Holle@vaisala.com

Heidi Huntrieser Deutsches Zentrum für Luft- und Raumfahrt (DLR), Institut für Physik der Atmosphäre, Oberpfaffenhofen, 82234 Wessling, Germany, heidi.huntrieser@dlr.de

Abram R. Jacobson Earth and Space Sciences, University of Washington, Seattle, Washington, USA

Dimitrios Katsanos Institute for Environmental Research and Sustainable Development, National Observatory of Athens, Greece, katsanos@meteo.noa.gr

Vassiliki Kotroni Institute for Environmental Research and Sustainable Development, National Observatory of Athens, Greece, kotroni@meteo.noa.gr

Yuriy Kuleshov National Climate Centre, Australian Bureau of Meteorology, GPO Box 1289K, Melbourne, Vic., 3001, Australia, Y.Kuleshov@bom.gov.au

Kostas Lagouvardos Institute for Environmental Research and Sustainable Development, National Observatory of Athens, Greece, lagouvar@meteo.noa.gr

Timothy L. Lang Colorado State University, Fort Collins, CO 80523, USA, tlang@atmos.colostate.edu

Tracy E. L. Light Space and Remote Sensing Group, ISR-2, Los Alamos National Laboratory, Los Alamos, New Mexico, USA

Marek Łoboda Department of High Voltage Engineering and Electrical Apparatus, Warsaw University of Technology, ul. Koszykowa 75, 00-665 Warsaw, Poland, marek.loboda@ien.pw.edu.pl

Jean-Yves Lojou Vaisala Inc, Tucson Operations, 2705 East Medina Road, Tucson, AZ 85706, USA, jean-yves.lojou@vaisala.com

Walter A. Lyons FMA Research, Inc, Fort Collins, CO 80524, USA, walyons@frii.com

David Mackerras School of Information Technology and Electrical Engineering, University of Queensland, and Lightning and Transient Protection Pty Ltd, Brisbane, Australia

Antti Mäkelä Finnish Meteorological Institute, P.O. Box 503, 00101 Helsinki, Finland, antti.makela@fmi.fi

Thomas C. Marshall Department of Physics and Astronomy, University of Mississippi, MS 38677-1848, USA, marshall@olemiss.edu

Jonathan D. Meyer FMA Research, Inc, Fort Collins, CO 80524, USA

Joan Montanya Department of Electrical Engineering, Technological University of Catalonia, Colon 1, 08222 Terrassa, Spain, montanya@ee.upc.edu

Alberto Mugnai Institute of Atmospheric Sciences and Climate, Italian National Research Council, Roma, Italy, a.mugnai@isac.cnr.it

Martin J. Murphy Vaisala Inc, Tucson Operations, 2705 East Medina Road, Tucson, AZ 85706, USA, martin.murphy@vaisala.com

Vadim Mushtak Massachusetts Institute of Technology, Parsons Laboratory, Cambridge, Massachusetts, USA, vadimcm@gmail.com

Kleber P. Naccarato Atmospheric Electricity Group – ELAT, Brazilian Institute of Space Research (INPE), S.J. Campos, Brasil, kleberp@dge.inpe.br

Thomas E. Nelson FMA Research, Inc, Fort Collins, CO 80524, USA

Wolf P. Oettinger nowcast GmbH, 81377 Munich, Germany

Kenneth Pickering NASA Goddard Space Flight Center, Laboratory for Atmospheres, Greenbelt, MD, USA, Kenneth.E.Pickering@nasa.gov

Nicolau Pineda Servei Meteorològic de Catalunya (Meteorological Service of Catalonia) C/Berlin 38–46, 08029 Barcelona, Spain, npineda@meteocat.com

Iara R.C.A. Pinto Atmospheric Electricity Group – ELAT, Brazilian Institute of Space Research (INPE), S.J. Campos, Brasil, iara@dge.inpe.br

Osmar Pinto Jr. Atmospheric Electricity Group – ELAT, Brazilian Institute of Space Research (INPE), S.J. Campos, Brasil, osmar@dge.inpe.br

Colin Price Tel Aviv University, Department of Geophysics and Planetary Science, Ramat Aviv, 69978, Israel, cprice@flash.tau.ac.il

Vladimir A. Rakov Department of Electrical and Computer Engineering, University of Florida, 553 Engineering Building #33, Gainesville, FL 32611-6130, USA, rakov@ece.ufl.edu

Steven A. Rutledge Colorado State University, Fort Collins, CO 80523, USA, Steven.Rutledge@colostate.edu

Marcelo M.F. Saba Atmospheric Electricity Group – ELAT, Brazilian Institute of Space Research (INPE), S.J. Campos, Brasil, msaba@dge.inpe.br

Gabriella Sátori Geodetic and Geophysical Research Institute, HAS, Csatkai u. 6–8, 9400 Sopron, Hungary, satori@ggki.hu

Kersten Schmidt Faculty of Physics, University of Munich, 85748 Garching, Germany

Serge Soula Université de Toulouse; UPS; LA (Laboratoire d'Aérologie); 14 avenue Edouard Berlin; F-31400 Toulouse CNRS; LA (Laboratoire d'Aérologie); F-31400 Toulouse

Mark A. Stanley FMA Research, Inc, Fort Collins, CO 80524, USA

Maribeth Stolzenburg Department of Physics and Astronomy, University of Mississipi, MS 38677-1848, USA, mstolzen@olemiss.edu

Sarah A. Tessendorf Research Applications Laboratory, National Center for Atmospheric Research, P.O. Box 3000, Boulder, CO 80307, USA, saraht@ucar.edu

Tapio J. Tuomi Finnish Meteorological Institute, P.O. Box 503, 00101 Helsinki, Finland, tapio.tuomi@fmi.fi

James A. Weinman Department of Atmospheric Sciences, University of Washington, Seattle, Washington, USA

Kyle C. Wiens Department of Geosciences, Texas Tech University, Lubbock, Texas, USA

Earle Williams Parsons Laboratory, Massachusetts Institute of Technology, Cambridge, Massachusetts, USA, earlew@ll.mit.edu

Chapter 1
Present Understanding of the Lightning Return Stroke

Yoshihiro Baba and Vladimir A. Rakov

Abstract In this chapter, a general picture of downward negative lightning discharges that take place between cloud and ground are described. Then, first and subsequent return strokes, which are the optically brightest processes and produce the most intense wideband electromagnetic signatures in the overall cloud-to-ground lightning discharge, referred to as the lightning flash, are presented. The first return stroke follows the path of initial downward-progressing stepped leader emerging from the cloud, and subsequent return strokes are usually initiated by dart leaders propagating downward along channels traversed by the preceding stroke(s). Representative models of lightning return strokes are also described.

Keywords Lightning flash · Return stroke · First stroke · Subsequent stroke · Stepped leader · Dart leader · Lightning return-stroke model

1.1 Introduction

Lightning discharges that take place between cloud and ground, referred to as cloud-to-ground lightning discharges, are classified, based on the polarity of the charge effectively transferred to ground and the direction of the initial leader, into four types. These are downward negative lightning, upward negative lightning, downward positive lightning, and upward positive lightning. The leader is a process that precedes the return stroke. It creates a conducting path between the cloud charge source and ground, and deposits charge along this path. It is believed that downward negative lightning discharges account for about 90% of all cloud-to-ground lightning, and that about 10% of cloud-to-ground lightning are downward positive lightning discharges. It is thought that upward lightning discharges occur only from tall objects (higher than 100 m or so) or from objects of moderate height located

Y. Baba (✉)
Department of Electrical Engineering, Doshisha University, 1-3 Miyakodani, Tatara, Kyotanabe, Kyoto 610-0321, Japan
e-mail: ybaba@mail.doshisha.ac.jp

H.D. Betz et al. (eds.), *Lightning: Principles, Instruments and Applications*,
DOI 10.1007/978-1-4020-9079-0_1,

on mountain tops. Note that terms, “lightning”, “the lightning discharge”, and “the lightning flash” are used interchangeably to refer to the overall lightning discharge process.

In this chapter, only downward negative lightning discharges are considered. This chapter is organized as follows. In Section 1.2, a general picture of downward negative lightning discharges to ground is presented. In Section 1.3, first return strokes that follow the path of initial downward-progressing stepped leader emerging from the cloud, and subsequent return strokes that are usually initiated by dart leaders propagating downward along channels conditioned by the preceding strokes are discussed. In Section 1.4, representative models of lightning return strokes are described.

1.2 General Picture of Downward Negative Lightning Discharges to Ground

In this section, a general picture of downward negative lightning flashes to ground is presented. Figure 1.1a and b schematically show still and time-resolved images of a downward negative lightning flash containing three strokes, respectively. Figure 1.1c shows the corresponding current at the channel base. In Figure 1.1b and c, time advances from left to right. Each of the three strokes is composed of a downward-moving process termed a leader and an upward-moving process termed a return stroke. The leader creates a conducting path between the cloud charge source and ground, and deposits negative charge along the path. The return stroke traverses the leader path upward from ground to the cloud charge source and neutralizes the negative leader charge. Thus, both leader and return-stroke processes contribute to transporting negative charge from the cloud to ground. The leader initiating the

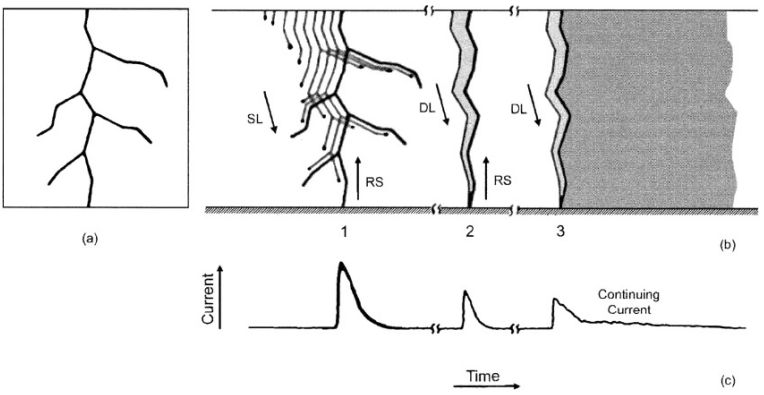

Fig. 1.1 Diagram showing the luminosity of a downward negative lightning flash to ground containing three strokes and the corresponding current at the channel base: (**a**) still image, (**b**) time-resolved image, and (**c**) channel-base current. Adapted from Rakov and Uman (2003)

first return stroke develops in virgin air, and appears to be an optically intermittent process. Therefore, it is termed "stepped leader". The stepped-leader branches are directed downward, which indicates that the stepped leader (and the flash) is initiated in the cloud and develops downward. The leaders initiating the two subsequent return strokes in Fig. 1.1 move continuously, as a downward-moving dart, along the pre-conditioned path of the preceding return stroke or strokes. Hence, these leaders are termed "dart leaders". Note that each downward negative lightning flash typically contains three to five strokes.

In the following, a sequence of the processes involved in a typical downward negative lightning flash is presented in more detail. The source of lightning is usually a thundercloud. The generally accepted features of the charge structure in the thundercloud include a net positive charge near the top, a net negative charge below it, and an additional positive charge at the bottom. The stepped leader is preceded by an in-cloud process called the initial breakdown or preliminary breakdown. There is no consensus on the mechanism of the initial breakdown. It can be viewed as a discharge process between the negative and lower positive charge regions, but it can also involve a sequence of channels extending in random directions from the cloud charge source. One of these events (in the case of multiple channels) evolves into the stepped leader which is a negatively charged plasma channel that bridges the cloud charge source and the ground. The stepped leader extends toward ground at an average speed of 2×10^5 m/s in a series of discrete steps, with each step being typically 1 μs in duration and tens of meters in length, with the interval between steps being 20–50 μs (e.g., Rakov and Uman 2003). The peak value of the current pulse associated with an individual step is inferred to be 1 kA or greater. Several coulombs of negative charge are distributed along the stepped-leader channel. The stepped-leader duration is typically some tens of milliseconds, and the average leader current is some hundreds of amperes. The stepped-leader channel is likely to consist of a thin core that carries the longitudinal channel current, surrounded by a corona sheath whose diameter is typically several meters.

As the stepped leader approaches ground, the electric field at the ground surface or objects increases until it exceeds the critical value for the initiation of upward connecting leaders. The initiation of an upward connecting leader from ground in response to the descending stepped leader marks the beginning of the attachment process. The process by which the extending plasma channels of the upward and downward leaders make contact, after forming common streamer zone, is called the break-through phase or final jump. The break-through phase can be viewed as a switch-closing operation that serves to launch two return-stroke waves from the point of junction between the two plasma channels. The length of an upward connecting leader involved in a first stroke is some tens of meters if that leader is launched from the ground, and it can be several hundred meters long if it is initiated from a tall object.

The return stroke serves to neutralize the leader charge, although it may not neutralize all the leader charge or may deposit some excess positive charge onto the leader channel and into the cloud charge source region. The speed of the return stroke, averaged over the visible channel, is typically between one-third and one-half

the speed of light (e.g., Rakov 2007). The speed decreases with increasing height, dropping abruptly after passing each major branch. The first return-stroke current measured at ground rises to an initial peak of about 30 kA in some microseconds and decays to half-peak value in some tens of microseconds while exhibiting a number of subsidiary peaks, probably associated with the branches (e.g., Rakov and Uman 2003). This impulsive component of current may be followed by a current of some hundreds of amperes lasting for some milliseconds. The return stroke effectively lowers to ground the several coulombs of charge originally deposited on the stepped-leader channel, including that on all the branches. The high-current return-stroke wave rapidly heats the channel to a peak temperature near or above 30,000 K and creates a channel pressure of 10 atm or more (e.g., Rakov and Uman 2003), which results in channel expansion, intense optical radiation, and an outward propagating shock wave that eventually becomes the thunder.

When the first return stroke ceases, the flash may end. In this case, the lightning is called a single-stroke flash. However, more often the residual first-stroke channel is traversed downwards by a leader that appears to move continuously, a dart leader. During the time interval between the end of the first return stroke and the initiation of a dart leader, J and K-processes occur in the cloud. The J-process is often viewed as a relatively slow positive leader extending from the flash origin into the negative charge region, the K-process then being a relatively fast "recoil streamer" that begins at the tip of the positive leader and propagates toward the flash origin. Both the J-processes and the K-processes in cloud-to-ground discharges serve to transport additional negative charge into and along the existing channel, although not all the way to ground. In this respect, K-processes may be viewed as attempted dart leaders. The processes that occur after the only stroke in single-stroke flashes and after the last stroke in multiple-stroke flashes are sometimes termed final (F) processes. These are similar, if not identical, to J-processes.

The dart leader progresses downward at a typical speed of 10^7 m/s, typically ignores the first stroke branches, and deposits along the channel a total charge of the order of 1 coulomb (e.g., Rakov and Uman 2003). The dart-leader current peak is about 1 kA. Some leaders exhibit stepping near ground while propagating along the path traversed by the preceding return stroke, these leaders being termed dart-stepped leaders. Additionally, some dart or dart-stepped leaders deflect from the previous return-stroke path, become stepped leaders, and form a new termination on the ground.

When a dart leader or dart-stepped leader approaches the ground, an attachment process similar to that described for the first stroke takes place, although it probably occurs over a shorter distance and consequently takes less time, the upward connecting-leader length being of the order of some meters. Once the bottom of the dart leader or dart-stepped leader channel is connected to the ground, the second (or any subsequent) return-stroke wave is launched upward and serves to neutralize the leader charge. The subsequent return-stroke current at ground typically rises to a peak value of 10–15 kA in less than a microsecond and decays to half-peak value in a few tens of microseconds. The upward propagation speed of such a subsequent return stroke is similar to or slightly higher than that of the first stroke (e.g.,

Rakov 2007). Note that due to the absence of branches the speed variation along the channel for subsequent return strokes does not exhibit abrupt drops. The radius of return-stroke channels is about 3 cm, the conductivity is about 10^4 S/m, and the resistance per unit length is about 0.035 Ω/m [$= 1/(10^4 \times \pi \times 0.03^2)$] (Rakov 1998).

The impulsive component of the current in a subsequent return stroke is often followed by a continuing current that has a magnitude of tens to hundreds of amperes and a duration up to hundreds of milliseconds. Continuing currents with a duration in excess of 40 ms are traditionally termed long continuing currents. Between 30 and 50 percent of all negative cloud-to-ground flashes contain long continuing currents. The source for continuing current is the cloud charge, as opposed to the charge distributed along the leader channel, the latter charge contributing to at least the initial few hundred microseconds of the return-stroke current observed at ground. Continuing current typically exhibits a number of superimposed surges that rise to a peak in some tens to hundreds of microseconds, the peak being generally in the hundreds of amperes range but occationally in the kiloamperes range. These current surges are associated with enhancements in the relatively faint luminosity of the continuing-current channel and are called M-components.

The time interval between successive return strokes in a flash is usually several tens of milliseconds, although it can be as large as many hundreds of milliseconds if a long continuing current is involved and as small as one millisecond or less. The total duration of a flash is typically some hundreds of milliseconds, and the total charge lowered to ground is some tens of coulombs. The overwhelming majority of negative cloud-to-ground flashes contain more than one stroke. Although the first stroke is usually a factor 2 to 3 larger than a subsequent stroke, about one-third of multiple stroke flashes have at least one subsequent stroke that is larger than the first stroke in the flash (e.g., Rakov et al. 1994).

1.3 First and Subsequent Lightning Return Strokes

In this section, parameters of lightning return-stroke currents, return-stroke wavefront propagation speeds, and generated electromagnetic fields are presented.

1.3.1 Lightning Return-Stroke Current

The most complete characterization of the lightning return stroke in the downward negative flash has been given by Berger et al. (1975). This characterization is based on oscillograms of current measured using resistive shunts installed at the tops of two 70-m high towers on the summit of a 915-m high mountain (above sea level). Since the mountain contributed to the electric field enhancement near the tower tops, the effective heights of the towers are considered to be several times greater than the actual tower heights. Therefore, the majority of lightning strikes to the towers was of the upward type. Here, only return strokes in downward negative flashes are

considered. It is important to note that Berger et al.'s direct current measurements for downward flashes are unique in that they were obtained over a period of more than 20 years, were continuous (that is, covering all processes in the flash), and were often accompanied by time-resolved optical records.

Figure 1.2 shows, on two time scales, A and B, the average impulsive current waveshapes for negative first and subsequent strokes. The rising portion of the first-stroke waveform has a characteristic concave shape. Figure 1.3 shows the cumulative statistical distributions (the solid curves) of return-stroke peak currents for (1) negative first strokes, (2) negative subsequent strokes, and (3) positive strokes (each of which was the only stroke in a flash), the latter not being further discussed here. These empirical results are approximated by log-normal distributions (the

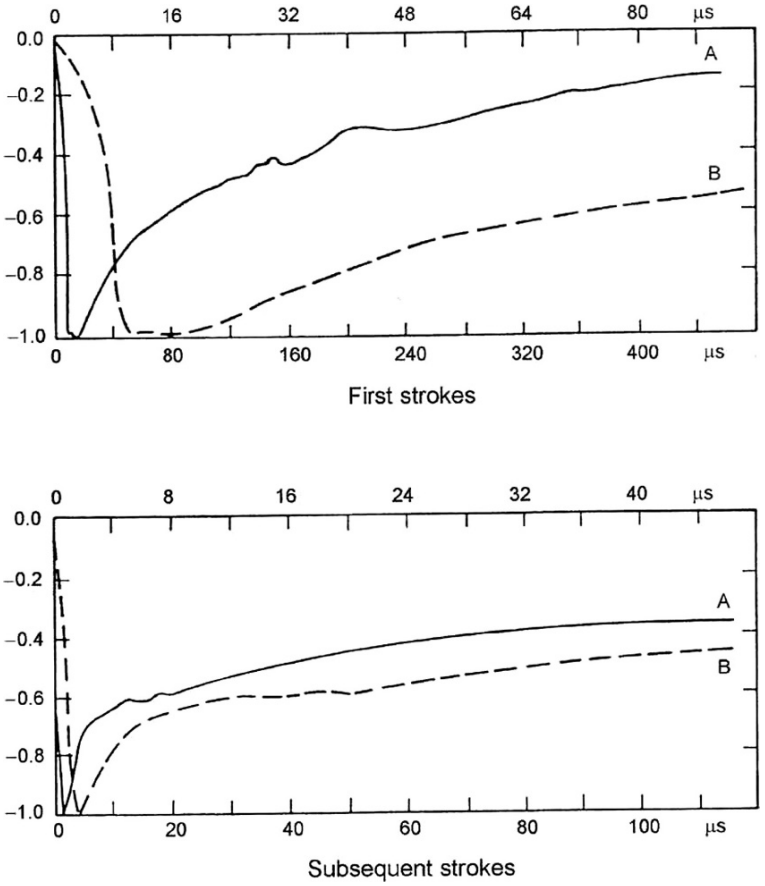

Fig. 1.2 Average negative first- and subsequent-stroke current each shown on two time scales, A and B. The lower time scales (**a**) correspond to the solid-line curves, while the upper time scales (**b**) correspond to the broken-line curves. The vertical scale is in relative units, the peak values being equal to negative unity. Adapted from Berger et al. (1975)

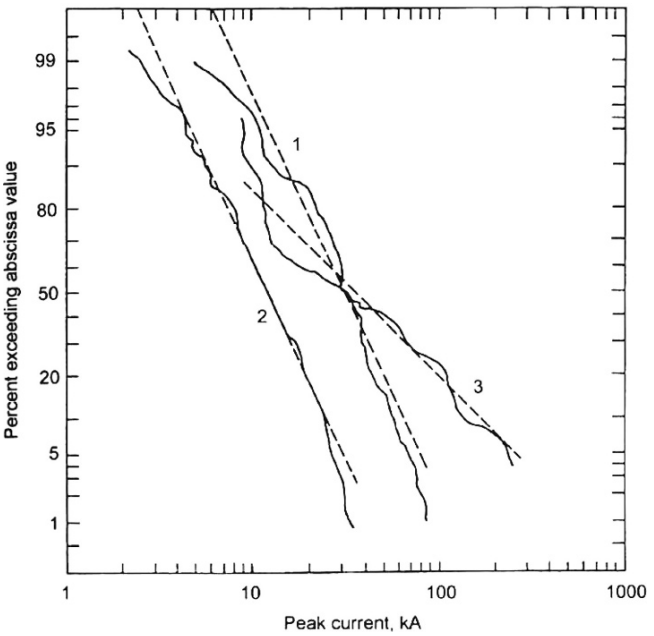

Fig. 1.3 Cumulative statistical distributions of return-stroke peak current from directr measurements at tower top (solid-line curves) and their log-normal approximations (broken lines) for (**1**) negative first strokes, (**2**) negative subsequent strokes, and (**3**) positive first (and only) strokes, as reported by Berger et al. (1975)

broken lines) and are given as they appear on cumulative-probability-distribution graph, on which a Gaussian cumulative distribution appears as a slanted straight line, the horizontal scale being logarithmic to base 10. The ordinate gives the percentage of peak currents exceeding the corresponding value on the horizontal axis. The lightning peak current distributions for negative first and subsequent strokes shown in Fig. 1.3 are characterized by 95, 50, and 5 percent values based on the log-normal approximations given in Table 1.1, which contains a number of other parameters derived from the current oscillograms. Note from Fig. 1.3 and Table 1.1 that the median return-stroke current peak for first strokes is two to three times higher than that for subsequent strokes. Also, negative first strokes transfer about a factor of four larger total charge than do negative subsequent strokes. On the other hand, subsequent return strokes are characterized by three to four times higher current maximum rate of rise. Note that the smallest measurable time in Berger et al.'s oscillograms was 0.5 μs versus the 95 percent value of 0.22 μs for the front duration for subsequent strokes in Table 1.1, which is a prediction of the log-normal approximation. Only a few percent of negative first strokes are expected to exceed 100 kA. The action integral in Table 1.1 represents the energy that would be dissipated in a 1-Ω resistor if the lightning current were to flow through it.

Table 1.1 Parameters of downward negative lightning derived from channel-base current measurements

Parameters	Units	Sample size	Percentage exceeding tabulated value		
			95%	50%	5%
Peak current (minimum 2 kA)	kA				
First stroke		101	14	30	80
Subsequent stroke		135	4.6	12	30
Charge (total charge)	C				
First stroke		93	1.1	5.2	24
Subsequent strokes		122	0.2	1.4	11
Complete flash		94	1.3	7.5	40
Impulse charge (excluding continuing current)	C				
First strokes		90	1.1	4.5	20
Subsequent strokes		117	0.22	0.95	4
Front duration (2 kA to peak)	μs				
First strokes		89	1.8	5.5	18
Subsequent strokes		118	0.22	1.1	4.5
Maximum dI/dt	kA μs^{-1}				
First strokes		92	5.5	12	32
Subsequent strokes		122	12	40	120
Stroke duration (2 kA to half peak value on the tail)	μs				
First strokes		90	30	75	200
Subsequent strokes		115	6.5	32	140
Action integral	A^{2}s				
First strokes		91	6.0×10^3	5.5×10^4	5.5×10^5
Subsequent strokes		88	5.5×10^2	6.0×10^3	5.2×10^4
Time interval between					
Strokes	ms	133	7	33	150
Flash duration	ms				
All flashes		94	0.15	13	1100
Excluding single-stroke		39	31	180	900
Flashes					

Source: Adapted from Berger et al. (1975).

1.3.2 Lightning Return-Stroke Luminosity Profile and Propagation Speed

Since the variation in current along the channel is impossible to measure directly, the luminosity profile along the channel is generally viewed as representative of the current variation.

When a first return stroke wavefront reaches a branch, there is usually a brightening of the channel below the point, this brightening being termed a branch component. Branch components are thought to be responsible for the secondary maxima

usually observed in the channel base current waveforms. Because of the lack of branches, the light profile along a subsequent return-stroke channel is relatively simple, usually showing a gradual intensity decay with height. Jordan et al. (1997) found that in two out of three events the return-stroke luminosity peak at 480 and 1400 m had decayed to, respectively, 70–75 percent and 25–30 percent of its value at the bottom of the channel and in the third event to, respectively, 90–95 percent and about 70 percent of the channel-bottom value.

Besides a decrease in peak value, the return-stroke light pulses also exhibit an appreciable increase in risetime with increasing height. Jordan et al. (1997) reported that the 20–80 percent risetime increased from 1.5 to 4.0 μs (mean values) as the return stroke propagated from ground to the cloud base at about 1400 m. Note that Wang et al. (2005) found from their comparative analysis for the channel-base current and light waveforms of rocket-triggered lightning strokes that the current and light signals had a remarkable linear relationship in their rising portions although the linearity disappeared after the peaks.

The average propagation speed of negative first or subsequent return stroke below the lower cloud boundary is typically between one-third and one-half of the speed of light (Rakov 2007). The speed usually decreases with height for both first and subsequent return strokes. There exists experimental evidence that the negative return-stroke speed may vary non-monotonically along the channel, initially increasing and then decreasing with increasing height. Note that the often assumed relationship between the return-stroke speed and peak current is generally not supported by experimental data.

1.3.3 Electric and Magnetic Fields Produced by Lightning Return Strokes

Typical vertical electric and horizontal magnetic field waveforms at distances ranging from 1 to 200 km for both first and subsequent strokes were published by Lin et al. (1979). These waveforms are drawings based on many measurements acquired in Florida and reproduced in Fig. 1.4. Four features have been identified by Nucci et al (1990) in these waveforms, which include (1) a sharp initial peak that varies approximately as the inverse distance beyond a kilometer or so in both electric and magnetic fields; (2) a slow ramp following the initial peak and lasting in excess of 100 μs for electric fields measured within a few tens of kilometers; (3) a hump following the initial peak in magnetic fields within a few tens of kilometers, the maximum of which occurs between 10 and 40 μs; and (4) a zero crossing within tens of microseconds of the initial peak in both electric and magnetic fields at 50–200 km.

The higher-frequency components of the return-stroke fields are preferentially attenuated in propagating over a finitely conducting earth (e.g., Lin et al. 1979; Cooray and Lundquist 1983). Lin et al. (1979) reported from two-station measurements that normalized field peaks were typically attenuated by 10 percent in propagating

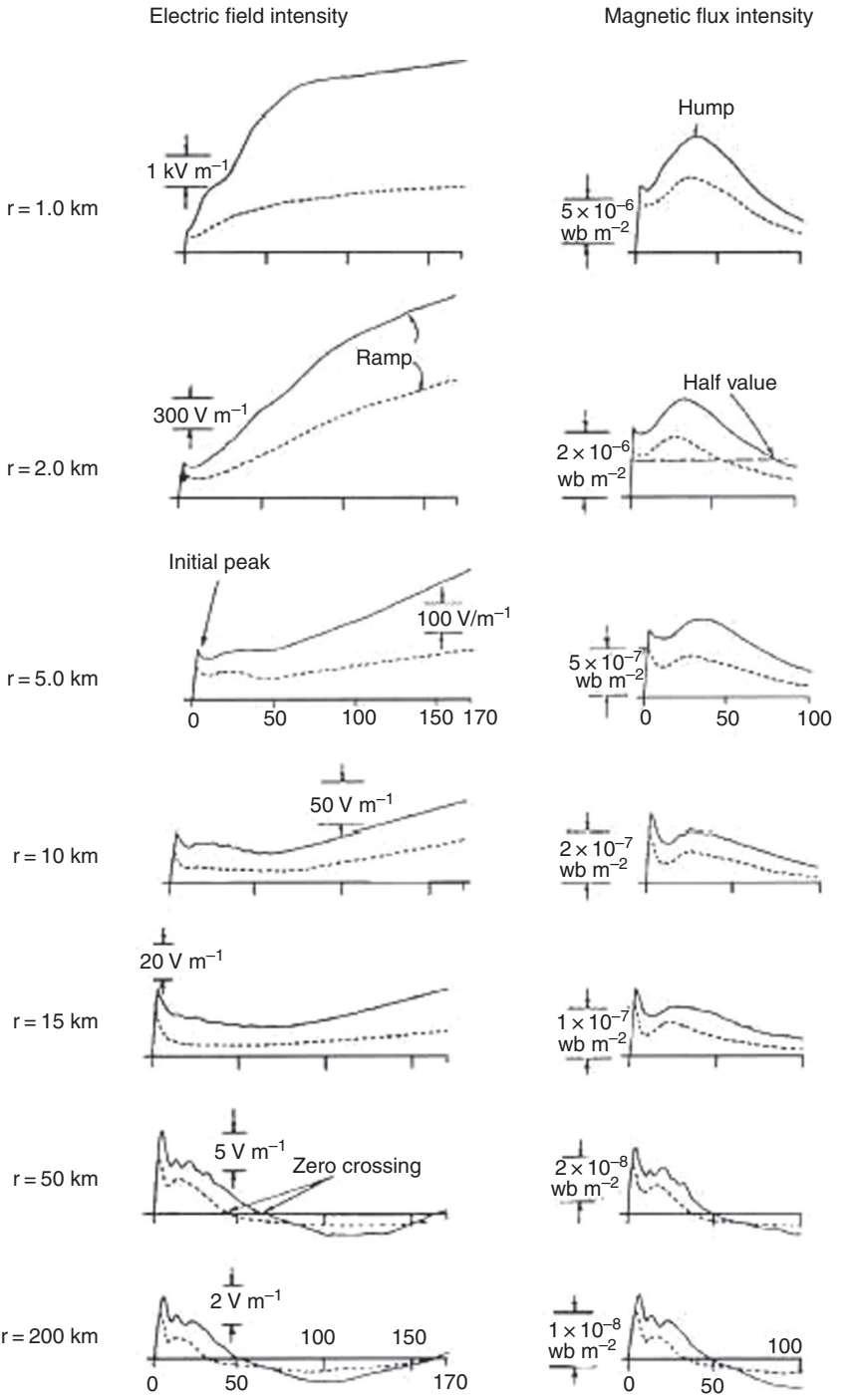

Fig. 1.4 Typical vertical electric field intensity (left column) and azimuthal magnetic flux density (right column) waveforms for first (solid line) and subsequent (broken line) return strokes at distances of 1, 2, 5, 10, 15, 50, and 200 km. The scales in the third row of diagrams from the top and in the bottom row of diagrams are in μs. Adapted from Lin et al. (1979)

over 50 km of Florida soil and 20 percent in propagating over 200 km. As to field risetimes, they are increased by an amount of order 1 μs in propagating 200 km across Florida soil for typical strokes (Uman et al. 1976).

1.4 Modeling of Lightning Return Strokes

In this section, classification of lightning return-stroke models is given and so-called engineering models are discussed. General equations for computing the vertical electric field and azimuthal magnetic field due to a lightning return-stroke current wave are presented.

1.4.1 Classification of Lightning Return-Stroke Models

Lightning return-stroke models are needed in studying lightning effects on various objects and systems and in characterizing the lightning electromagnetic environment. Rakov and Uman (1998), based on governing equations, have categorized return-stroke models into four classes: gas dynamic models, electromagnetic models, distributed-circuit models, and "engineering" models.

Gas dynamic models are primarily concerned with the radial evolution of a short segment of the lightning channel and its associated shock wave. These models typically involve the solution of three gas dynamic equations representing the conservation of mass, momentum, and energy, coupled to two equations of state with the input being an assumed channel current versus time (e.g., Plooster 1971). Principal model outputs include temperature, pressure, and mass density as a function of radial coordinate and time.

Electromagnetic models are based on a lossy, thin-wire antenna approximation to the lightning return-stroke channel. In this class of models, Maxwell's equations are solved to yield the distribution of current along the lightning channel using numerical techniques. These models allow a self-consistent full-wave solution for both current distribution along the lightning channel and associated electromagnetic fields. They have attracted considerable attention during the last ten years or so (e.g., Baba and Rakov 2007).

Distributed-circuit models of the lightning return stroke usually consider the lightning channel as an *R-L-C* transmission line (e.g., Gorin 1985; Rakov and Uman 1998), where *R*, *L*, and *C* are series resistance, series inductance, and shunt capacitance, all per unit length, respectively. In an *R-L-C* transmission line model, voltage and current are the solutions of the telegrapher's equations.

Engineering models prescribe the longitudinal current along the lightning channel, based on the existing knowledge on evolution of return-stroke waveform as it propagates from ground toward the cloud (e.g., Nucci et al. 1990; Rakov and Uman 1998). The return-stroke wavefront speed in these models can be set arbitrarily since it is one of the input parameters.

Note that the so-called hybrid electromagnetic/circuit (HEM) model (e.g., Visacro and Silveira 2004), which employs electric scalar and magnetic vector potentials for taking account of electromagnetic coupling but is formulated in terms of circuit quantities, voltages and currents, occupies an intermediate place between electromagnetic and distributed-circuit models.

1.4.2 Representative Engineering Return-Stroke Models

Out of four or five classes of lightning return-stroke models, the class of engineering models is most widely used. An engineering return-stroke model is an equation that relates the longitudinal channel current $I(z',t)$ at any height z' and any time t to the current $I(0,t)$ at the channel origin ($z' = 0$). A number of simple engineering models can be expressed by the following equation:

$$I\left(z',t\right) = u\left(t - z'/v_f\right) P\left(z',t\right) I\left(0, t - z'/v\right) \tag{1.1}$$

where u is the Heaviside function equal to unity for $t \geq z'/v_f$ and zero otherwise, $P(z',t)$ is the height- and time-dependent current attenuation factor, v_f is the upward-propagating front speed, and v is the current-wave propagation speed. Table 1.2 summarizes $P(z',t)$ and v for five engineering models, the transmission-line model (TL) (Uman and McLain 1969); the modified transmission-line model with linear current decay with height (MTLL) (Rakov and Dulzon 1987); the modified transmission-line model with exponential current decay with height (MTLE) (Nucci et al. 1988); the modified transmission-line model with linear current decay and dispersion with height (MTLD) (Baba and Ishii 2002); and the traveling current source model (TCS) (Heidler 1985). The Diendorfer and Uman model (DU) (Diendorfer

Table 1.2 Height- and time-dependent current attenuation factor $P(z',t)$ and the current-wave propagation speed v in Eq. (1.1), $I(z', t) = u(t\text{-}z'/v_f)P(z', t)I(0,t\text{-}z'/v)$, for five simple engineering return-stroke models. Note that $I(z',t)$ is the longitudinal channel current at any height z' and any time, $I(0,t)$ is the longitudinal current at the channel origin ($z' = 0$), v_f is the upward-propagating front speed, and u is the Heaviside function equal to unity for $t \geq z'/v_f$ and zero otherwise

Model	$P(z',t)$	v
TL (Uman and McLain 1969)	1	v_f
MTLL (Rakov and Dulzon 1987)	$1-z'/H$	v_f
MTLE (Nucci et al. 1988)	$\exp(-z'/\lambda)$	v_f
MTLD (Baba and Ishii 2002)	$\left[1 - \exp\left(-\frac{t - z'/v_f}{\tau}\frac{\lambda_p}{z'}\right)\right]\left(1 - \frac{z'}{H}\right)$	v_f
TCS (Heidler 1985)	1	$-c$

H is the total channel height for the MTLL model, λ is the current decay constant for the MTLE model (it is assumed to be $\lambda = 2000$ m in Nucci et al. (1998)), and c is the speed of light. For the MTLD model, $\tau(z'/\lambda_p)$ controls the risetime of the channel current (the risetime increases with increasing the height z'), and $(1\text{-}z'/H)$ controls the attenuation of the channel current. Baba and Ishii (2002) assumed that $\tau = 0.3$ μs, $\lambda_p = 1000$ m.

and Uman 1990) can be expressed by the following extension of Eq. (1.1) for the TCS model ($P(z',t) = 1$, $v = -c$):

$$I\left(z',t\right) = u\left(t - \frac{z'}{v_f}\right)\left[I\left(0, t + \frac{z'}{c}\right) - I\left(0, \frac{z'}{v_f} + \frac{z'}{c}\right)\exp\left(-\frac{t - z'/v_f}{\tau_D}\right)\right] \tag{1.2}$$

where τ_D is the discharge time constant. It is usually assumed that $\tau_D = 0.6$ μs or so. Note that Diendorfer and Uman (1990) used a current waveform given as the sum of two currents, each of which is given by Eq. (1.2) but has a different discharge constant, in order to match model-predicted fields with measured fields. One of the two time constants is for breakdown current and its value is assumed to be 0.6 μs, and the other is for corona current and its value is assumed to be 5 μs (Diendorfer and Uman 1990).

The TL, MTLL, MTLE, and MTLD models are the TL-type models, and the TCS and DU models are the TCS-type models. The TL-type models can be viewed as incorporating a current source at the channel base. This is why they are also referred to as lumped-source (LS) models. The source injects a specified current wave into the channel, that wave propagating upward without either dispersion or attenuation in the TL model, without dispersion but with specified attenuation in the MTLL and MTLE models, or with both specified dispersion and attenuation in the MTLD model. The conceptual illustration for the TL model and waveforms of current at different heights along the vertical lightning channel calculated for the TL model are shown in Figs. 1.5a and 1.6, respectively.

The TCS-type models can be viewed as incorporating a current source at the wavefront, which moves upward with speed v_f and injects a current wave into the

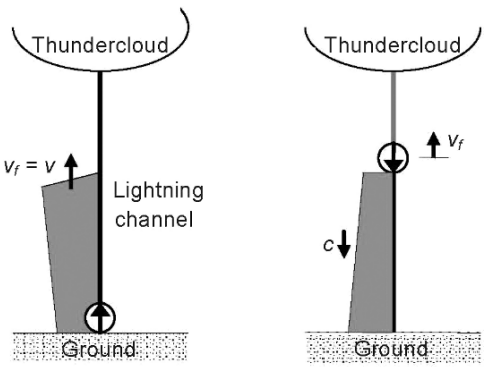

Fig. 1.5 Conceptual illustrations of (**a**) the TL model and (**b**) the TCS model. In the TL model, a current source incorporated at the channel base injects a specified current wave into the channel, and the current wave propagates upward with speed $v = v_f$ without either dispersion or attenuation. In the TCS model, a current source at the wavefront moves upward with speed v_f, and injects a current wave into the channel that propagates downward at speed c

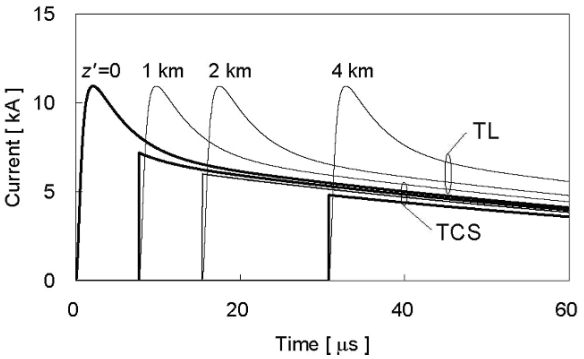

Fig. 1.6 Waveforms of current at different heights along the vertical lightning return-stroke channel calculated for the TL and TCS models. The channel-base current waveform, $I(0, t)$, is characterized by a magnitude of 11 kA and a 10-to-90% risetime of 1 μs. The return-stroke front speed is set to $v_f = 130$m/μs. Current in the TCS model exhibits a discontinuity at the upward-moving wavefront

channel that propagates downward at speed c (see Fig. 1.5b). In the TCS model, current at a given channel section turns on instantaneously as this section is passed by the front, and therefore this model exhibits an inherent discontinuity at the upward-moving wavefront. In the DU model (see Eq. (1.2)), the first term is the same as the downward-propagating current in the TCS model, and the second term is an opposite polarity current which rises instantaneously to the value equal in magnitude to the current at the wavefront and then decays exponentially with a time constant τ_D. The second current component in the DU model eliminates any current discontinuity at the wavefront. The conceptual illustration for the TCS model and waveforms of current at different heights along the vertical lightning channel calculated for the TCS model are shown in Figs. 1.5b and 1.6, respectively. TCS-type models can be also represented by current sources distributed along the lightning channel and progressively activated by upward-moving return-stroke front. Therefore, they can be viewed as distributed-source (DS) models, as suggested by Maslowski and Rakov (2007).

Cooray (2003) showed that any LS model can be formulated in terms of sources distributed along the lightning channel. This has been previously demonstrated for one model (MTLE) by Rachidi and Nucci (1990). The approach suggested by Cooray (2003) was used by Rachidi et al. (2002) to generalize five engineering models in order to take into account a tall strike object. It has been recently shown by Maslowski and Rakov (2007) that any engineering return-stroke model can be expressed using an appropriate continuity equation in terms of either lumped or distributed current sources with the resultant longitudinal current distribution (and total charge density distribution) along the channel being the same. This property can be viewed as the duality of engineering models. Lumped-source (LS)-type and distributed-source (DS)-type models are illustrated in Fig. 1.7a and b, respectively. Both longitudinal (upward or downward propagating wave) and radial corona (sinks or sources) currents are shown in this Figure. The conversion alters the actual corona

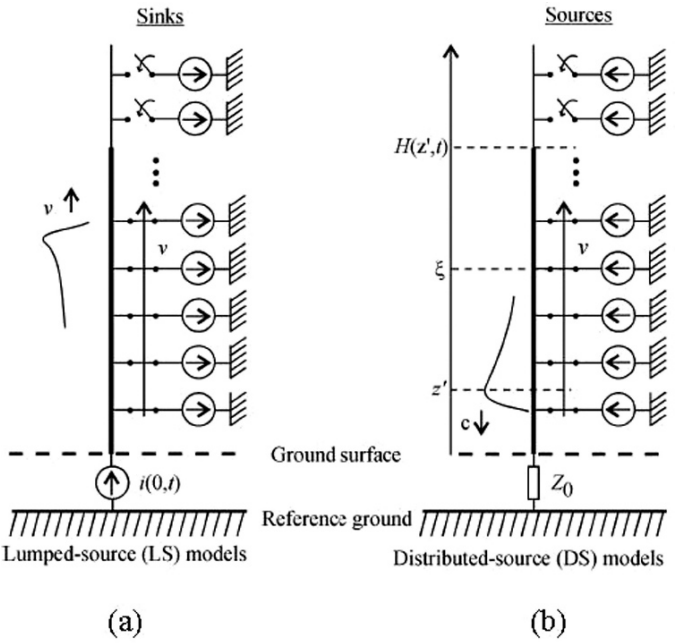

Fig. 1.7 Schematic illustration of engineering return-stroke models that employ (**a**) a lumped current source at the lightning channel base (LS-type models) and (**b**) distributed current sources along the channel (DS-type models). v is the upward return-stroke front speed, c is the speed of light, and Z_0 is the characteristic impedance of the lightning channel (matched conditions at ground are implied in DS-type models). LS-type models with longitudinal-current decay with height imply current sinks distributed along the channel, as shown in (**a**). Adapted from Maslowski and Rakov (2007)

current (if any) of the model. For LS-type models, the actual corona current is unipolar and directed radially out of the channel core, while for DS-type models it is unipolar and directed into the channel core. For LS-type models converted to DS-type models, the corona current is the sum of the negated actual corona current and a fictitious corona current, the later being bipolar. For the TL model (no longitudinal-current attenuation with height) expressed in terms of distributed sources, there is only a fictitious bipolar corona current component. Conversion of the TCS model to its equivalent LS-type model involves replacement of the actual, unipolar corona current with a fictitious one, the latter current being bipolar near the channel base and unipolar at higher altitudes.

Baba et al. (2004) proposed a modification to the DU model, which could reproduce all the four features identified in measured waveforms and listed in Section 1.3.3 and one additional feature, a characteristic flattening within 15 μs or so of vertical electric fields observed at tens to hundreds of meters from triggered lightning strokes (Rakov and Uman 1998). This model (modified DU model with additional decay, referred to as the MDUD model here) is expressed by

$$I_{MDUD}\left(z',t\right) = I_{DU}\left(z',t\right)\left[1-\exp\left(-\left(\lambda_d/z'\right)^n\right)\right] \tag{1.3}$$

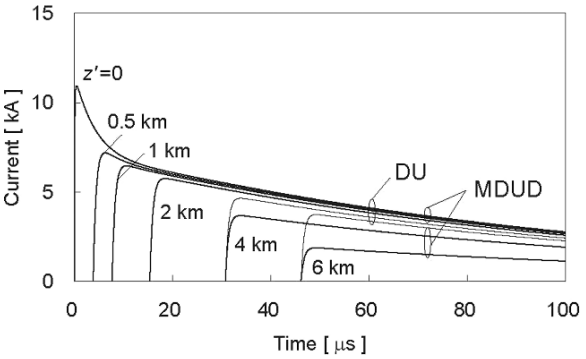

Fig. 1.8 Waveforms of current at different heights along the vertical lightning channel calculated for the DU and MDUD models. The channel-base current waveform, $I(0, t)$, is characterized by a magnitude of 11 kA and a 10-to-90% risetime of 0.15 μs. The return-stroke front speed is set to $v_f = 130$ m/μs. In the DU model, Eq. (1.2), the discharge time constant is set to $\tau_D = 0.6$ μs. In the MDUD model, Eq. (1.3), λ_d and n are set to 5000 m and 2, respectively. When these values of input parameters are used, the magnitude of the MDUD model current is reduced, relative to that in the DU model, to about 80 and 50% at heights $z' = 4$ and 6 km, respectively, while it is essentially the same as that for the DU model at heights below $z' = 2$ km

where $I_{DU}(z',t)$ is the channel current given by Eq. (1.2). The recommended constant values are $\lambda_d = 5000$ m and $n = 2$. When these constant values are used, the magnitude of the MDUD model current is reduced, relative to that in the DU model, to about 80 and 50% at heights $z' = 4$ and 6 km, respectively, while it is essentially the same as the DU model current at heights below $z' = 2$ km. Figure 1.8 shows waveforms of current at different heights along the vertical lightning channel calculated for the DU and MDUD models. The channel-base current waveform, $I(0, t)$, is characterized by a magnitude of 11 kA and a 10-to-90% risetime of 0.15 μs.

1.4.3 Equations for Computing Electric and Magnetic Fields

The most general equations for computing the vertical electric field E_z and azimuthal magnetic field B_φ due to an upward-moving return stroke for the case of an observation point P on perfectly conducting ground (see Fig. 1.9) are given by Thottappillil et al. (1997) and reproduced below.

$$\begin{aligned} E_z(r,t) = {} & \frac{1}{2\pi\varepsilon_0}\int_0^{H(t)} \frac{2z'^2 - r^2}{R^5(z')} \int_{\frac{z'}{v_f}+\frac{R(z')}{c}}^{t} I\left(z', \tau - R\left(z'\right)/c\right) d\tau dz' \\ & + \frac{1}{2\pi\varepsilon_0}\int_0^{H(t)} \frac{2z'^2 - r^2}{cR^4(z')} I\left(z', \tau - R\left(z'\right)/c\right) dz' \\ & - \frac{1}{2\pi\varepsilon_0}\int_0^{H(t)} \frac{r^2}{c^2 R^3(z')} \frac{\partial I\left(z', t - R\left(z'\right)/c\right)}{\partial t} dz' \\ & - \frac{1}{2\pi\varepsilon_0} \frac{r^2}{c^2 R^3(H(t))} I\left(H(t), v_f\right) \frac{\mathrm{d}H(t)}{\mathrm{d}t} \end{aligned} \tag{1.4}$$

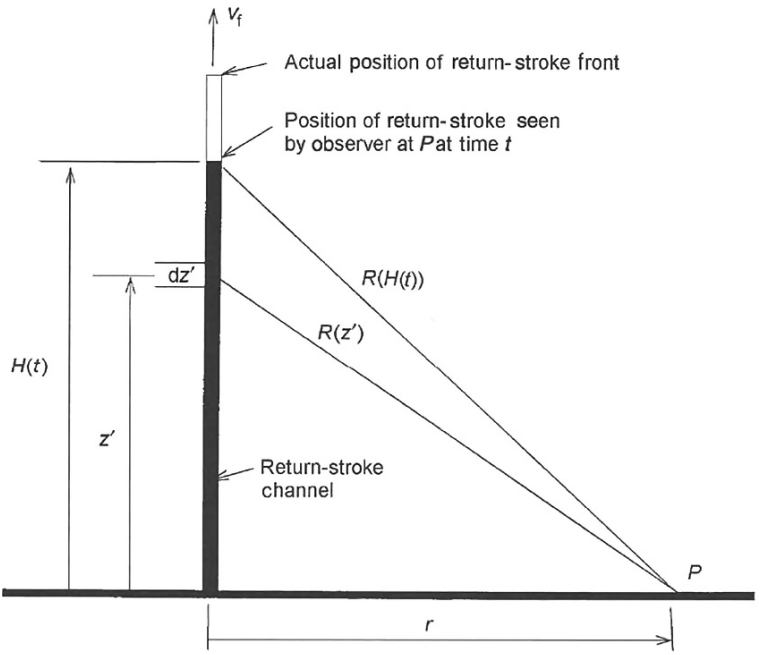

Fig. 1.9 Geometry used in deriving equations for the electric and magnetic fields at a point P on perfectly conducting ground at a horizontal distance r from the vertical lightning return-stroke channel extending upward with speed v_f. Adapted from Thottappillil et al. (1997)

$$B_\varphi(r,t)=\frac{\mu_0}{2\pi}\int_0^{H(t)}\left[\frac{r}{R^3(z')}I\left(z',t-R\left(z'\right)/c\right)+\frac{r}{cR^2(z')}\frac{\partial I\left(z',t-R\left(z'\right)/c\right)}{\partial t}\right]dz'$$
$$+\frac{\mu_0}{2\pi}\frac{r}{cR^2(H(t))}I\left(H(t),H(t)/v_f\right)\frac{\mathrm{d}H(t)}{\mathrm{d}t} \qquad (1.5)$$

where $I(z', t)$ is the current along the vertical lightning channel at height z' and time t, and $H(t)$ is the height of the front as seen by the observer at time t. This height can be found from the equation, $t = H(t)/v_f + R(H(t))/c$. $I(z', t)$ can be specified by electromagnetic, distributed-circuit, or engineering lightning return-stroke model.

The first three terms in Eq. (1.4), traditionally referred to as the electrostatic, induction, and electric radiation field components, respectively, and the first two terms in Eq. (1.5), referred to as the magnetostatic (or induction) and magnetic radiation field components, respectively, describe the field due to sources below the upward-moving front. The last term in each of these two equations accounts for a possible current discontinuity at the moving front. The front discontinuity produces only a radiation field component, no electrostatic or induction field components.

Figure 1.10a, b, and c show waveforms of vertical electric field on the surface of perfectly conducting ground at horizontal distances $r = 50$ m, 5 km, and 100 km from the vertical lightning channel, calculated using Eq. (1.4) for the MDUD